Stray-field NMR imaging and wavelength dependence of optically pumped nuclear spin polarization in InP

Carl A. Michal and Robert Tycko
Laboratory of Chemical Physics, National Institute of Diabetes and Digestive and Kidney Diseases, National Institutes of Health, Bethesda, Maryland 20892-0520
(Received 16 April 1999)

One-dimensional NMR imaging experiments with micron spatial resolution are used to investigate the penetration depth and excitation energy dependence of optical pumping in Fe-doped semi-insulating InP crystals in high magnetic field at low temperature. The depth profile of ^{31}P nuclear polarization revealed by NMR imaging is consistent with previous optical absorption measurements, while the efficiency of exciting nuclear polarization is found to be a complicated function of the excitation energy. This dependence is not explained by LO phonon emission by the photoexcited carriers. The optically pumped ^{31}P NMR signal exhibits a maximum intensity with excitation several meV below the band gap, but this maximum is shown to be due to the dramatically increased absorption length of below-gap radiation. The efficiency of exciting nuclear polarization drops off quickly below the gap, and is about $\frac{1}{5}$ of its maximum value at the energy of greatest total NMR signal intensity. [S0163-1829(99)14735-0]

I. INTRODUCTION

Optical pumping of nuclear spin polarization in a semiconductor was first observed by direct detection of nuclear magnetic resonance (NMR) signals in silicon. Lampel[1] showed that irradiation with circularly polarized, near band-gap light could drive the ^{29}Si spin temperature away from thermal equilibrium, greatly enhancing the NMR signal. Further studies by Bagraev *et al.*[2–4] showed that larger nuclear spin polarizations could be produced by optical pumping in Si samples with deep donor impurities. Many studies have since been performed on III-V direct-gap semiconductors, primarily GaAs and GaAs/$Al_xGa_{1-x}As$ heterostructures.[5–19] The strong photoluminescence from these materials allows the detection of nuclear polarization and NMR spectra to be performed optically[20] as first demonstrated by Ekimov and Safarov.[5] Optical detection is performed by measuring the degree of circular polarization of the luminescence as a function of applied rf frequency. Optical detection offers the advantage of significantly greater sensitivity, but is limited to samples with polarized luminescence and to experiments in relatively low magnetic fields. Direct NMR detection, in contrast, does not require polarized luminescence or high luminescence quantum yields, is compatible with high fields, and is particularly well suited to the observation of ground-state NMR spectra and NMR signals of nuclei that lack direct electron couplings.[16–18] Direct detection of optically pumped NMR signals has proven to be especially useful in studies of two-dimensional electron systems in GaAs quantum wells.[16–18,21,22]

Optical pumping of electron spin polarization in InP was first reported by Weisbuch and Lampel.[23] Evidence of optically pumped nuclear spin polarization in InP was first obtained in optically-detected electron nuclear double resonance (ENDOR)[24] and electron spin resonance (ESR)[25] measurements of the P_{In} antisite, and has since been observed directly.[26–29] As has been recently noted,[27] the details of electron-nuclear spin interactions under optical pumping conditions are not well established. This is especially true in high magnetic field. As an example, we have recently reported the unexpected excitation of nuclear dipolar order by optical pumping in InP.[28,29] Other studies have begun to demonstrate the role of variables such as temperature, magnetic field, and excitation power on the nuclear polarization obtained in both GaAs (Ref. 30) and InP.[26]

Measurements of the excitation energy dependence of the nuclear polarization in variously doped crystals of GaAs by Pietrass *et al.*[19] revealed that the greatest NMR signal enhancement was achieved with photon energies less than the bulk semiconductor band gap. It was suggested that this was due to the direct photoexcitation of shallow states (traps or excitons) below the band gap combined with an increase in the effective sample size by the deeper penetration of the light at below-gap energies, but the two effects could not be separated. In this paper, we report measurements of optically-pumped ^{31}P NMR spectra of InP made in a stray-field NMR imaging configuration where the effects of light penetration into the sample may be deconvoluted from the wavelength-dependent efficiency of optical pumping. Stray-field imaging permits one-dimensional spatial resolution approaching 1 μm. To our knowledge, this is the first use of magnetic resonance imaging to study penetration effects or to probe the spatial distribution of optically pumped spin polarization in a semiconductor. We also present high-resolution measurements of the excitation energy dependence of the NMR signal enhancement for σ^+ and σ^- light where we find behavior significantly different from that observed in GaAs. The experiments described below are motivated by our interest in transferring optically pumped nuclear polarization from ^{31}P to surface species in an organic overlayer to enhance the NMR signals obtained from small organic and biological samples.[26] Because ^{31}P is a naturally abundant spin-$\frac{1}{2}$ nucleus with a relatively large magnetogyric ratio, InP is likely to be a suitable substrate for transferred optical pumping experiments.[26]

II. PRINCIPLES

The deep cooling of nuclear spins that occurs under optical pumping conditions in semiconductors is generally believed to occur by Overhauser cross-relaxation from photoexcited electrons trapped on donors.[8] Near-gap circularly polarized light excites spin-polarized conduction electrons and holes. The polarization of photoexcited holes is generally ignored when considering nuclear polarization because the hole spin-relaxation is very fast ($\sim 10^{-12}-10^{-13}$ s) (Ref. 31) and the hole wave functions are composed of p orbitals, which have little contact-hyperfine coupling to the nuclei. The possible contribution of hole spin polarization to optical pumping of nuclear spins has not been excluded experimentally, however, particularly in high magnetic field. The initial electron polarization depends on the details of the band structure and the initial and final electron state,[32] but can differ substantially from thermal equilibrium, reaching a maximum value of ± 0.5 (Ref. 33). The steady-state electron polarization also depends upon the leakage of polarization through spin relaxation, and may be written

$$P_e = P_0 \frac{\tau_s}{\tau + \tau_s} = -\frac{n_+ - n_-}{n_+ + n_-}, \tag{1}$$

for undoped and p-type samples. P_0 is the average electron spin at the instant of excitation, τ_s is the electron spin relaxation time, and τ is the electron lifetime. n_+ and n_- are the number of electron spins parallel and antiparallel to the applied field and the sign reflects the convention that for electrons with positive g factor, the n_- state has lower Zeeman energy than n_+. The steady-state polarization thus depends on the ratio of τ/τ_s, which can vary widely depending upon the sample temperature and the concentration of defects and impurities. In p-type InP, τ_s and τ have been recently estimated as 2.7 and 9.3 ns, respectively.[27] We also note that the equilibrium electron polarization may be affected by spin-dependent recombination, which can be responsible for increasing the steady-state polarization; electronic polarizations up to 70% have been observed.[34] While the above is correct for conduction electrons, nuclear polarization arises from trapped electrons. Measurements of the photoluminescence polarization in GaAs suggest large ($r \sim 100$ Å),[7] shallow trapping sites which are in rapid spin-exchange with the conduction-band electrons. Measurements to date in InP are less transparent. Mao *et al.*[25] find nuclear polarization generated at deep P_{In} antisites where the wave function is very highly localized,[24] essentially within the first two neighbor shells. More recent measurements[27] suggest that nuclear polarization occurs at more than one type of trapping site.

Polarization is transferred to the nuclei by fluctuating contact-hyperfine couplings (and possibly dipolar-hyperfine couplings as well[28]) at the electronic trapping sites. The steady-state nuclear polarization will be affected by the loss of polarization to nuclear relaxation processes and, assuming contact-hyperfine interaction in the short correlation time limit and a spin-$\frac{1}{2}$ nucleus, may be written

$$P_N = \frac{T_1}{T_1 + T_{1e}} \tanh\left\{\frac{\hbar}{2k_B}\left[\frac{\omega_N}{T} \mp \left(\frac{\omega_e}{T_e} - \frac{\omega_e}{T}\right)\right]\right\} + \frac{T_{1e}}{T_1 + T_{1e}} \tanh\left(\frac{\hbar\omega_N}{2k_B T}\right), \tag{2}$$

where T_{1e} is the nuclear spin relaxation time due to the trapped electron, T_1 is the nuclear spin relaxation time due to other processes, $\omega_N = \gamma_N B_0$ is the nuclear resonance frequency, $\omega_e = g^* \mu_B B_0/\hbar$ is the electron resonance frequency, g^* is the effective g factor for the electron trap site, T is the lattice temperature, and T_e and T_N are the steady-state electron and nuclear spin temperatures, defined through $P_i = \tanh(\hbar\omega_i/2k_B T_i)$ for $i = e, N$ and the upper sign should be taken when the electron g factor and nuclear γ have the same sign.

If $T_1 \gg T_{1e}$, Eq. (2) simplifies to

$$\frac{1}{T_N} - \frac{1}{T} = \mp \frac{\omega_e}{\omega_N}\left(\frac{1}{T_e} - \frac{1}{T}\right), \tag{3}$$

where, because $\omega_e/\omega_N \sim 10^3$, it becomes clear that a small deviation from thermal equilibrium of the electron spin polarization may bring about a very low-nuclear spin temperature.

For ^{31}P nuclei with positive γ, a positive g factor ($g = 1.26$ for conduction electrons in InP) (Ref. 35) would suggest that σ^+ light produces an enhanced electron polarization, i.e., a small positive electron spin temperature, which in turn will generate a large negative nuclear spin polarization (small negative T_N). Conversely, σ^- light will generate either a negative or large positive T_e in turn generating a large positive nuclear spin polarization (small positive T_N). This is the behavior that is observed in Fe-doped semi-insulating InP (Ref. 28) but opposite to that seen in undoped InP (Ref. 26). While measurements of g factors for both the P_{In} antisite[25] and the Fe^{3+} impurity[36] reveal values close to 2, it is possible that the dominant contribution to nuclear spin polarization in undoped samples occurs at some as yet unidentified site with negative g factor. This point underscores the incomplete level of understanding of the underlying physics.

In GaAs, the transfer of polarization occurs fairly rapidly ($T_{1e} \sim 80$ ms) (Ref. 8) within a Bohr radius of the trap site, but polarization of nuclei farther away occurs only through the relatively slow process of spin diffusion. Nuclear spin diffusion rates in semiconductors are generally of the order of 10^{-13} cm^2/s (Ref. 8), implying the polarization of volumes of dimensions of a few 100 Å in 100 s. For pumping times up to the order of the bulk nuclear T_1 then, the amplitude of the nuclear resonance signal will continue to build as polarization diffuses into the spaces between the pumping sites.

III. EXPERIMENT

A 0.5 cm square sample of 348 μm thick (100) orientation Fe-doped semi-insulating InP (Showa Denko lot 60706) was etched in a 1% Br_2/Methanol solution for 4 h before mounting on a sapphire substrate with Apiezon N grease. The substrate had grooves cut in one face to allow a four turn NMR coil of 0.4-mm copper wire to encircle the sample while maintaining thermal, but not electrical contact with the cold finger of a customized Janis Supertran-B cryostat. The cryostat was equipped with the rotary motion feedthroughs, variable capacitors, and coaxial feedthroughs required for operation as a low temperature NMR probe. The sample

temperature was controlled with a Lakeshore model 805 temperature controller and was measured with a carbon glass resistor embedded in the cryostat cold finger. All experiments in this paper were carried out with the cold finger at 6 K unless otherwise indicated.

Laser light from a Spectra Physics 3900S Ti:Sapphire laser pumped with a Spectra Physics Millenia V Nd:YVO_4 laser was reflected from the laser table down to an optical rail which extended beneath the 9.39 T, 89 mm bore (Oxford Instruments, UK) magnet. The light passed through a spectrometer controlled shutter and through two lenses, which could be positioned to adjust the size of the laser spot on the InP surface. A window in the bottom of the cryostat allowed light to strike the sample after reflection off a 45° mirror directly below the magnet bore. The laser light propagated parallel to the magnetic field in all experiments. The spot size was measured with a linear array charge-coupled device detector by removing the 45° mirror. Circular polarization was generated with a zero-order quarter-wave plate in the beam path following the final reflection. The absolute sense of the circular polarization could be determined from the orientation of the laser's linear polarization and the location of the slow axis of the quarter-wave plate, and was verified by comparison with the circular polarization produced by a Fresnel rhomb. Laser powers up to ~ 1 W were available over the wavelength range of interest and were measured at the laser with a Spectra Physics model 407A laser power meter. Approximately 80% of the measured power was delivered to the sample. Wavelengths were measured with an Inst-rees laser spectrum analyzer.

^{31}P NMR measurements were made with a Chemagnetics/Varian Infinity-400 NMR spectrometer. With the sample in the magnet center, spectra were acquired with the pulse sequence: SAT-τ_L-τ_D-$\pi/2$-DET in which SAT is a train of 64 $\pi/2$ pulses separated by 1 ms, used to destroy any initial ^{31}P polarization, τ_L is a period of time during which the shutter is open and the sample is illuminated, τ_D is a period during which the shutter is closed, and DET represents the detection of a free-induction-decay following the $\pi/2$ pulse. The $\pi/2$ pulse length was approximately 2.4 μs with 200 W of rf power. The ^{31}P NMR frequency was 161.6 MHz in the magnet center. For imaging measurements, the cryostat was raised so that the sample was positioned outside of the magnet center, where field gradients up to 4.53 kG/cm (780 Hz/μm) were obtained. The cryostat was supported on an aluminum plate equipped with leveling screws so that the orientation of the sample could be adjusted. The experimental arrangement for stray-field imaging is shown in Fig. 1. In this imaging configuration, the following spin-echo pulse sequence was used to eliminate distortions due to the receiver dead-time: SAT-τ_L-τ_D-$\pi/2$-τ_E-π-τ_E-DET where τ_E represents an echo delay during which the sample is in darkness. In all measurements $\tau_D = 1$ s and $\tau_E = 50$ μs. All data were apodized with 2500 Hz Gaussian line broadening.

IV. RESULTS

^{31}P NMR spectra acquired with the sample in the magnet center are displayed in Fig. 2. The spectra acquired with shorter τ_L [Figs. 2(e)–2(f)] display a mixed absorptive and emissive character as a consequence of dipolar order generated during optical pumping.[28] Because the characteristic build-up time for dipolar order is on the order of 15 s, while the build-up time for Zeeman order is much longer, the spectra acquired with longer τ_L Fig. 2(c)–2(d) appear purely emissive, as compared to spectra acquired without optical pumping Fig. 2(a). All of the imaging experiments utilized a pumping time of 120 s to ensure that the acquired line shapes reflected only the spatial distribution of nuclear spin polarization and were not distorted by the presence of dipolar

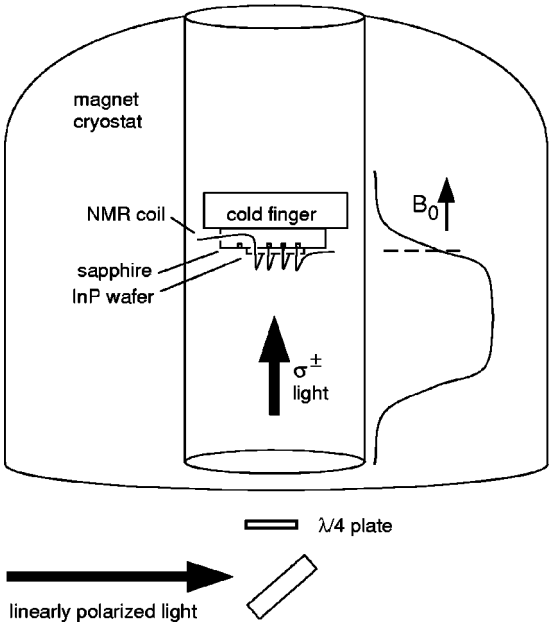

FIG. 1. Experimental configuration for stray-field imaging. The cryostat surrounding the sample assembly has been omitted for clarity. The curve on the right depicts the static field profile of the magnet, with the dashed line indicating the position of the sample.

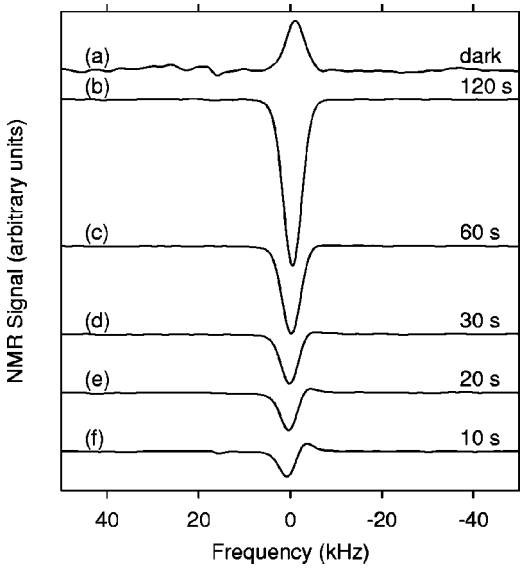

FIG. 2. Dependence of ^{31}P NMR signal line shape on pumping time. Spectra acquired with saturation-recovery sequence as described in text. (a) spectrum acquired with $\tau_L = 0$ and $\tau_D =$ 600 s. (b)–(f) with the τ_L indicated, $\tau_D = 1$ s, 0.8 W σ^+ polarized light at 1.418 eV, 3.7-mm diameter spot size. All spectra processed identically and on the same vertical scale.

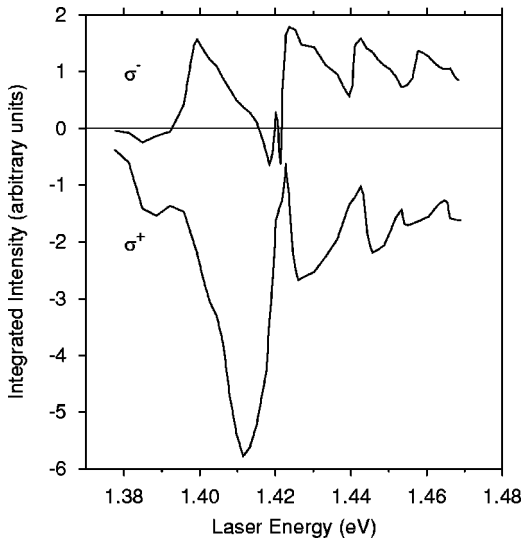

FIG. 3. Dependence of integrated ^{31}P NMR signal intensity on laser excitation energy and polarization. Measurements made in zero-field gradient with a single acquisition using the saturation-recovery pulse sequence with $\tau_L = 60$ s, $\tau_D = 1$ s, 0.5-W laser power in a 3.7-mm diameter spot.

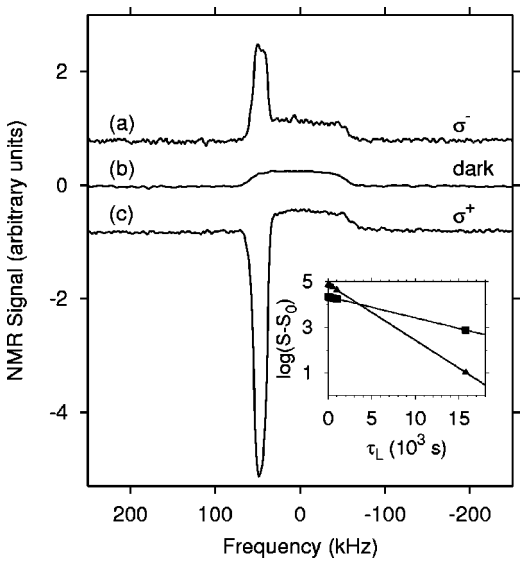

FIG. 4. One-dimensional ^{31}P NMR images of InP acquired with the saturation-recovery spin-echo pulse sequence described in text. The laser power was 0.2 W in a 3.7-mm diameter spot. (a) $\tau_L = 600$ s, $\tau_D = 0$ s 1.413 eV (b) $\tau_L = 0$ s, $\tau_D = 57\,000$ s, sample temperature $= 20$ K. (c) $\tau_L = 15\,800$ s, $\tau_D = 0$ s, 1.430 eV. The vertical scales in (b) and (c) are the same. Inset: estimate of relaxation times for the configuration corresponding to (c). Triangles correspond to the integrals of negative signals from the illuminated surface (35 to 70 kHz), fit to $S_0[1-\exp(-t/T_1)]$ with $T_1 = 4090$ s. Squares correspond to the integrals of the positive signals from the bulk of the sample (-70 to 35 kHz) and are fit with $T_1 = 10\,800$ s.

nuclear spin order. The spectra with $\tau_L = 60$ and 120 s are well fit with a simple Gaussian lineshape with full-width 4200 Hz (before apodization). This line shape is due primarily to ^{31}P-^{115}In dipolar and pseudodipolar couplings.[37,38] The residual field gradient at the sample position is $\ll 1$ G/cm.

The dependence of the ^{31}P NMR signal intensity as a function of excitation energy and polarization are shown in Fig. 3. The largest peak in the NMR intensity is observed with excitation energies below the band gap with σ^+ polarization. The exact position of the band gap in InP is somewhat uncertain, as there are large discrepancies among various measurements, with recent values ranging from 1.424–1.432 eV (Ref. 39).

Figure 4 displays stray-field NMR images acquired with the sample 12 cm above the magnet center, in a field gradient of 335 Hz/μm (1.95 kG/cm) at a ^{31}P resonance frequency of 130.2 MHz, both in the dark and with circularly polarized light. These are relatively low-resolution images that permit the entire InP wafer thickness to be displayed within the NMR excitation bandwidth. In Figs. 4(a) and 4(c), the lower surface of the sample is illuminated. Optical pumping produces the large positive or negative peaks at the high-frequency edge of the image. The relatively large width ($\sim$15 kHz) of the leading edges is due to a slight misorientation of the sample with respect to the field gradient and does not indicate the depth of optically pumped nuclear polarization in this case. A 15 kHz linewidth would be expected from a 45-μm vertical displacement over the laser spot of 3.7 mm, which requires just a 0.7° misalignment of the sample. These spectra show clearly the difference in behavior of the illuminated surface from the bulk of the sample. The nuclear spin relaxation times observed from the illuminated surface and the bulk of the sample are also dramatically different. The inset of Fig. 4 shows the integrated intensity of the two regions as a function of τ_L under σ^+ illumination. The relaxation times extracted from these measurements are 4090 s and 10 800 s for the surface and bulk, respectively.

To measure the depth of sample that contributes to the optically pumped NMR signals, high-resolution one-dimensional images were obtained by raising the sample further to 17 cm above the magnet center, where the field gradient is 780 Hz/μm (4.53 kG/cm) and the ^{31}P resonance is at 130.2 MHz. The sample orientation was adjusted to minimize the NMR linewidth observed with a large (3.7 mm) laser spot with excitation at 1.427 eV. To increase the spatial resolution further, the laser spot size was reduced to 0.45 mm. Images acquired in this configuration as a function of excitation energy are displayed in Fig. 5. The asymmetric broadening of the images as the photon energy decreases from above (1.427 eV) to below (1.403 eV) the InP band gap demonstrates the increasing depth of optical pumping. These data are fitted to simulations that assume an exponential penetration profile into the sample, convoluted with a Gaussian line broadening. The calculations were corrected for the effects of the finite length rf pulses used to excite NMR signals. The Gaussian line broadening used in the simulations included contributions from three sources. The first is from the natural dipolar linewidth of the sample (4200 Hz). The second contribution (2500 Hz) reflects the apodization applied to the experimental data in processing. The third contribution is due to the finite laser spot size and sample misorientation (explained further below). The only other free parameters in the fits are the NMR frequency at the illuminated surface, and the overall amplitude and phase of the NMR signals. Both the real and imaginary part of the spectrum are calculated and utilized in the fit. The amplitude

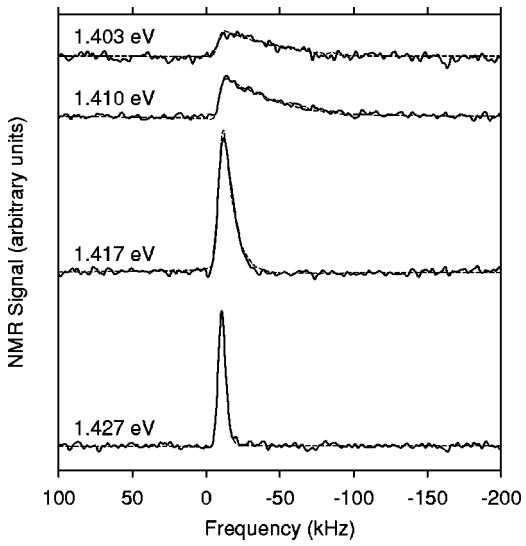

FIG. 5. High-resolution ^{31}P NMR images with 25 mW σ^+ light in a 0.45-mm spot as a function of photon energy. Data collected with the saturation-recovery spin-echo pulse sequence with $\tau_L = 120$ s and $\tau_D = 1$ s. Each spectrum is the result of four acquisitions except for that at 1.403 eV, which represents eight. The sign of the signals is inverted relative to Figs. 2–4 (i.e., all signals here are emissive).

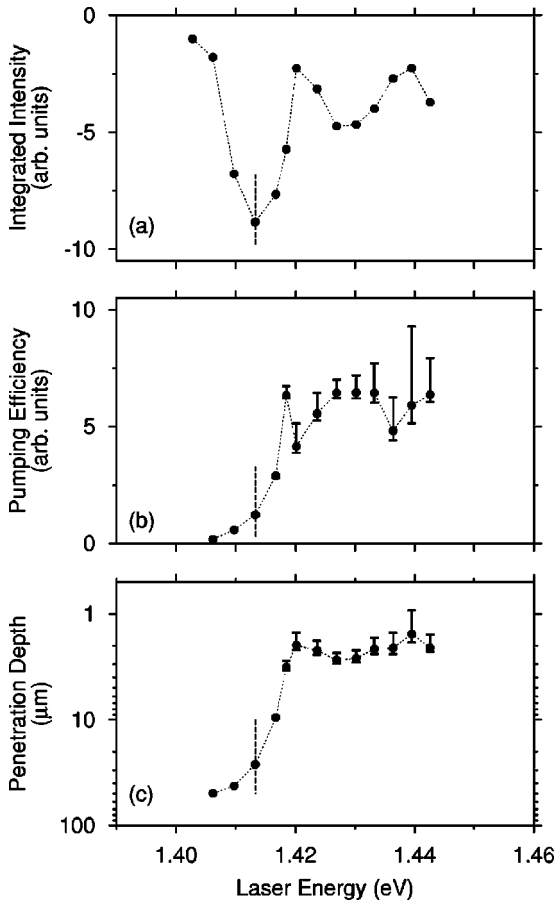

FIG. 6. Parameters extracted from high-resolution images: (a) total integrated intensity, (b) optical pumping efficiency and (c) penetration depth. In (b) and (c), the error bars represent the range of best fits found by assuming sample tilt angles from 0.1° to 0.4°. Filled circles assume a 0.25° tilt angle. All spectra acquired with 25 mW σ^+ light in a 0.45-mm diameter spot.

extracted from the fit is taken to be the pumping efficiency, i.e., the amplitude of nuclear spin polarization at the surface produced per unit volume of sample with fixed pumping time and power.

The total integrated intensity, pumping efficiency, and penetration depth as functions of excitation energy obtained from the fits are displayed in Fig. 6. The error bars and filled circles in Figs. 6(b) and 6(c) are from best fits obtained assuming sample misorientations of 0.1, 0.25, and 0.4°. These values contribute linewidths of 610, 1530, and 2450 Hz, respectively to the overall Gaussian width. Performing fits with the misorientation contribution as a free parameter yielded values in this range.

The laser energy of the absorption edge is shifted by approximately 7 meV from the measurements of Turner *et al.*,[40] most likely due to strain associated with the mounting of our sample. We observe a weak local minimum in the penetration depth at an energy similar to the exciton peak found in those measurements. There is also a dramatic peak in the optical pumping efficiency at a slightly lower energy still. The line drawn through the pumping efficiency data is a guide to the eye only, as we expect that higher energy resolution measurements would yield structure similar to that in Fig. 3, where the total integrated intensity is plotted versus energy at much higher energy resolution with the sample in the magnet center.

The largest peak in the total ^{31}P NMR signal intensity [indicated with a vertical dashed line in Fig. 6(a)] occurs at lower energy than the peak in the pumping efficiency. In fact, the pumping efficiency is approximately 20% of its maximum value at the energy of the maximum total intensity, demonstrating that this peak is due to the increased penetration depth at this lower energy.

To estimate the maximum nuclear polarization achieved with long pumping times, we allowed the sample to come to thermal equilibrium in the dark at 20 K, acquiring a spectrum with 5° pulses every 1400 s following an initial saturation of any ^{31}P magnetization. A similar measurement of the emissive signal obtained with a 3.7-mm diameter laser spot, 0.8-W laser power at 1.430 eV (above the absorption edge), and the cold finger at 6 K for a total of 2.0×10^4 s gave a signal -5.65 times the 20 K thermal equilibrium signal. The equilibration time used was greater than four times the effective T_1 value of the illuminated surface of the sample, but only about twice the T_1 of the bulk. This signal thus includes a fully relaxed emissive component from the surface as well as a partially relaxed absorptive component from the bulk of the sample. Assuming the emissive component arises from the top 2 μm (best fit penetration depth determined from the imaging experiments), and adjusting for the partially relaxed absorptive component (a 30% correction), we find the polarization at the surface to be -0.28. The fact that the laser beam does not cover the entire sample surface would slightly increase the maximum value, as we have assumed uniform horizontal polarization. The largest uncertainty by far however, comes from the penetration depth measurement itself; if instead we insert the 0.8 μm absorption length from Turner *et al.*,[40] we find a surface polarization of -0.70. For comparison, polarizations of -0.033 were reported[16] for

^{71}Ga nuclei in an *n*-doped GaAs/Al_xGa_{1-x}As multiple quantum well structure with a 30 s pumping time. In our samples, 30 s pumping time would yield a polarization between -0.002 and -0.005, depending on the penetration depth assumed.

V. DISCUSSION

The principal result of these experiments is that the optical pumping efficiency is far less than its maximum value at the position of the total intensity maximum. Efforts to transfer nuclear polarization from optically-pumped ^{31}P nuclei to surface species in an organic overlayer[26] will be aided by knowledge that the surface nuclear polarization is substantially greater at higher energy.

The data of Fig. 6 suggest a minimum penetration depth in the range 0.9–2.6 μm, in qualitative agreement of the 0.8 μm observed by direct optical absorption measurements.[40] While diffusion of spin-polarized electrons from the surface into the bulk may be responsible for our measurement of penetration depths slightly larger than those determined from optical absorption, the penetration depths derived from the fits should be taken as an upper bound, as any mechanism that contributes to broadening of the resonance line will increase the extracted value. Such broadening may arise from sources such as vibration of the sample, magnet, or optics, or instability of the laser source.

The use of high incident light power density could lead to an increase in the apparent penetration depths if the power density is great enough that all optical pumping sites near the surface are fully occupied. In this case, we would expect a deviation from the exponential penetration profile according to

$$P(z)=P_S\left[1-\exp\left(-\frac{I_0}{I_S}e^{-z/z_0}\right)\right], \tag{4}$$

where z is the depth, P_S is the saturation signal amplitude, I_0 is the incident intensity, I_S is the saturation intensity, and z_0 is the optical absorption depth. Even though our power levels (~ 4 W/cm^2) are much greater than the saturation values observed previously [~ 0.1 W/cm^2 in *n*-doped GaAs/Al_xGa_{1-x}As quantum wells[16] and undoped InP (Ref. 26)] the data of Fig. 5 are well fit with the simple exponential shape. In addition, the total integrated intensities observed in the imaging configuration and at the magnet center are in good agreement after scaling by the total incident laser powers, even though the incident power density is a factor of three greater for the imaging configuration. Again, this suggests the absence of saturation of optical pumping in the imaging configuration. The previous saturation value[26] was estimated on a nominally undoped sample. It is possible that the Fe doping in our present sample provides more pumping sites and explains a difference in saturation power level. The nature of the optical pumping sites has not been conclusively established. Evidence that nuclear polarization in Zn-doped InP occurs at P_{In} antisite defects[25] suggests that nuclear polarization may occur at a variety of defects and impurities, and not just on shallow donors. The fact that the sign of the nuclear spin polarization generated by a given helicity of light is reversed between undoped[26] and Fe-doped semi-insulating samples (this paper and Ref. 28) suggests that the iron impurities do play some role in the nuclear spin polarization process. Recent photomagnetization measurements on Mn-doped InP (Ref. 41) demonstrate the possibility for optically-oriented electrons to magnetize Mn impurities in the InP lattice. In that work it was suggested that a similar phenomenon may occur in Fe-doped InP.

The nuclear spin relaxation times obtained for the surface and bulk of the sample are significantly different from the T_1 measurements made in the dark. T_1 is a sensitive function of the temperature, and was found to be 2.0×10^4 s at 20 K, and 4.1×10^4 s at 8 K in the dark. These T_1 values for our Fe-doped sample are substantially longer than those reported for other types of samples (6740 s for undoped[26] and 310 s for *n*-doped[42] at 13.8 and 4.2 K respectively). While some sample heating is possible due to the laser irradiation, measurements of the sample temperature in a similar configuration made with a sensor mounted directly on the surface suggest no more than a 2–3 K increase at this power level. Therefore, sample heating does not account for the reduction in T_1 in the bulk. Another possibility is that spin-relaxed photoexcited electrons in the sample bulk could be responsible for relaxing nuclear spins there. Such carriers could diffuse from the illuminated surface, or be generated within the bulk by photon recycling.[43] Electron diffusion lengths in illuminated semi-insulating InP at low temperature in high field are not well characterized, but we note that luminescence from photoexcited carriers have been observed from as deep as 40 μm beneath the surface.[43]

The sawtooth shape of the dependence of the total ^{31}P NMR signal intensity on excitation energy (Fig. 3) is intriguing. We do not have a conclusive explanation for these results, but two possibilities merit discussion. Although similar measurements on bulk GaAs have shown a single peak just below the band gap,[19] our present data are reminiscent of the oscillations with energy observed from GaAs/Al_xGa_{1-x}As multiple quantum wells.[16] In that work the oscillations were due to the two-dimensional confinement of electrons within the 300-Å wide GaAs wells. The excitation energy of the light then corresponded to differences in energy between discrete two-dimensional electron and hole energy levels. While there is no fabricated quantum well structure in our samples, surface band bending can produce a confining potential.[44] Quantum confinement effects are expected if the confinement length is less than the electron de Broglie wavelength, $\lambda=h(3m_e^*k_BT)^{-1/2}=0.15$ μm for thermalized electrons at 6 K in InP. This seems an unlikely explanation here, as the data demonstrate optical pumping effects on length scales set by the optical absorption length.

We suspect that the shape of Fig. 3 is due to the details of the electron momentum relaxation. Because the nuclear polarization arises from trapped electrons,[8] those carriers excited with $k>0$ must relax before they can participate in polarizing nuclei. The emission of LO phonons is known to occur very rapidly (~ 100 fs) (Ref. 45) and is in some cases the principal mechanism of energy and momentum relaxation.[46] Peaks corresponding to LO phonon emission have been observed in the photoluminescence polarization (representing electron spin orientation) as a function of excitation energy in CdS.[47] Similar peaks corresponding to emission of mixtures of optical and acoustic phonons were ob-

served in GaSb.[48] Our data bear a marked resemblance to the photomagnetization measurements made on the narrow gap system $Hg_{1-x}Mn_xTe$.[49,50] In that work sawtooth shaped onset behavior was observed in the photomagnetization as a function of excitation energy. The data were well simulated with a model featuring LO phonon emission.

Peaks are expected to be found at energies where $(h\nu - E_g)/(1+m_e^*/m_h^*) = n\hbar\omega_{LO}$. In InP, $\omega_{LO} = 42$ meV,[51,52] $m_e^* = .079m_0$, $m_{hh} = 0.60m_0$, and $m_{lh} = 0.12m_0$.[53] These values suggest peak spacings of 47 meV for electrons excited from heavy holes, and 70 meV for those from light holes. These spacings are much larger than the separations between peaks in our measurements, which range from $\sim 8-22$ meV, therefore LO phonon emission cannot account for our results. TA and LA phonon sidebands have been observed in the photoluminescence of Fe-doped InP.[36,54] The energies of TA and LA zone-boundary phonons range between 5 and 23 meV (Ref. 52), which appears to be more compatible with our data.

Other explanations for these results are certainly possible, and further experimentation will be necessary for a complete understanding.

VI. CONCLUSIONS

We have performed one-dimensional NMR imaging experiments to investigate the penetration depth and excitation energy dependence of optical pumping in Fe-doped InP crystals. We find that the laser energy dependent nuclear polarization profile extends to depths similar to those suggested by previous optical absorption measurements, but that the amount of nuclear polarization produced has a complicated dependence on energy, which is not explained by previously observed mechanisms. The greatest total nuclear polarization and total NMR signal are achieved with below-gap energies where a decrease in the optical pumping efficiency is offset by the deeper penetration, which greatly expands the effective sample volume. An estimate of the nuclear polarization produced at the surface of the sample suggests ^{31}P polarizations in the tens of percent may be obtained with pumping times of the order of hours.

The imaging experiments show conclusively that the surface polarization for moderate pumping times is greatest at laser energies near or above the band gap, and not at the below-gap energy where the largest total NMR signal is observed.

[1] G. Lampel, Phys. Rev. Lett. **20**, 491 (1968).

[2] N. T. Bagraev, L. S. Vlasenko, and R. A. Zhitnikov, Fiz. Tverd. Tela **19**, 2504 (1977) [Sov. Phys. Solid State **19**, 1467 (1977)].

[3] N. T. Bagraev and L. S. Vlasenko, Zh. Éksp. Teor. Fiz. **75**, 1743 (1978) [Sov. Phys. JETP **48**, 878 (1978)].

[4] N. T. Bagraev and L. S. Vlasenko, Fiz. Tverd. Tela **21**, 120 (1979) [Sov. Phys. Solid State **21**, 70 (1979)].

[5] A. I. Ekimov and V. I. Safarov, Pis'ma Zh. Éksp. Teor. Fiz. **15**, 453 (1972) [JETP Lett. **15**, 319 (1972)].

[6] D. Paget, G. Lampel, B. Sapoval, and V. I. Safarov, Phys. Rev. B **15**, 5780 (1977).

[7] D. Paget, Phys. Rev. B **24**, 3776 (1981).

[8] D. Paget, Phys. Rev. B **25**, 4444 (1982).

[9] V. K. Kalevich, V. L. Korenev, and O. M. Fedorova, Pis'ma Zh. Éksp. Teor. Fiz. **52**, 964 (1990) [JETP Lett. **52**, 349 (1990)].

[10] G. P. Flinn, R. T. Harley, M. J. Snelling, A. C. Tropper, and T. M. Kerr, Semicond. Sci. Technol. **5**, 533 (1990).

[11] M. Krapf, G. Denninger, H. Pascher, G. Weimann, and W. Schlapp, Solid State Commun. **78**, 459 (1991).

[12] S. K. Buratto, D. N. Shykind, and D. P. Weitekamp, Phys. Rev. B **44**, 9035 (1991).

[13] S. K. Buratto, D. N. Shykind, and D. P. Weitekamp, J. Vac. Sci. Technol. B **10**, 1740 (1992).

[14] S. K. Buratto, J. Y. Hwang, N. D. Kurur, D. N. Shykind, and D. P. Weitekamp, Bull. Magn. Reson. **15**, 190 (1993).

[15] J. A. Marohn, P. J. Carson, J. Y. Hwang, M. A. Miller, D. N. Shykind, and D. P. Weitekamp, Phys. Rev. Lett. **75**, 1364 (1995).

[16] S. E. Barrett, R. Tycko, L. N. Pfeiffer, and K. W. West, Phys. Rev. Lett. **72**, 1368 (1994).

[17] S. E. Barrett, G. Dabbagh, L. N. Pfeiffer, K. W. West, and R. Tycko, Phys. Rev. Lett. **74**, 5112 (1995).

[18] R. Tycko, S. E. Barrett, G. Dabbagh, L. N. Pfeiffer, and K. W. West, Science **268**, 1460 (1995).

[19] T. Pietraß, A. Bifone, T. R$\tilde{o}\tilde{o}$m, and E. L. Hahn, Phys. Rev. B **53**, 4428 (1996).

[20] V. G. Fleisher and I. A. Merkulov, in *Optical Orientation*, edited by F. Meier and B. Zakharchenya (North-Holland, Amsterdam, 1984), Chap. 5, pp. 173–258.

[21] P. Khandelwal, N. N. Kuzma, S. E. Barrett, L. N. Pfeiffer, and K. W. West, Phys. Rev. Lett. **81**, 673 (1998).

[22] N. N. Kuzma, P. Khandelwal, S. E. Barrett, L. N. Pfeiffer, and K. W. West, Science **281**, 686 (1998).

[23] C. Weisbuch and G. Lampel, *11th International Conference on the Physics of Semiconductors* (PWN-Polish Scientific Publishers, Warsaw, 1972), pp. 1327–1333.

[24] D. Y. Jeon, H. P. Gislason, J. F. Donegan, and G. D. Watkins, Phys. Rev. B **36**, 1324 (1987).

[25] D. Mao, P. C. Taylor, and W. D. Ohlsen, Phys. Rev. B **49**, 7952 (1994).

[26] R. Tycko, Solid State Nucl. Magn. Reson. **11**, 1 (1998), special issue.

[27] W. Farah, M. Dyakonov, D. Scalbert, and W. Knap, Phys. Rev. B **57**, 4713 (1998).

[28] C. A. Michal and R. Tycko, Phys. Rev. Lett. **81**, 3988 (1998).

[29] R. Tycko, Mol. Phys. **95**, 1169 (1998).

[30] C. R. Bowers, Solid State Nucl. Magn. Reson. **11**, 11 (1998), special issue.

[31] C. Hermann, G. Lampel, and V. I. Safarov, Ann. Phys. (Paris) **10**, 1117 (1985).

[32] M. I. Dyakonov and V. I. Perel, in *Optical Orientation* (Ref. 20), Chap. 2, pp. 11–71.

[33] R. R. Parsons, Phys. Rev. Lett. **23**, 1152 (1969).

[34] C. Weisbuch, J. Phys. Colloq. **35**, C3-21 (1974).

[35] C. Weisbuch and C. Hermann, Solid State Commun. **16**, 659 (1975).

[36] W. H. Koschel, U. Kaufmann, and S. G. Bishop, Solid State Commun. **21**, 1069 (1977).

[37] M. Engelsberg and R. E. Norberg, Phys. Rev. B **5**, 3395 (1972).

[38] M. Tomaselli, D. deGraw, J. L. Yarger, M. P. Augustine, and A. Pines, Phys. Rev. B **58**, 8627 (1998).
[39] L. Pavesi, F. Piazza, A. Rudra, J. F. Carlin, and M. Ilegems, Phys. Rev. B **44**, 9052 (1991).
[40] W. J. Turner, W. E. Reese, and G. D. Pettit, Phys. Rev. **136**, A1467 (1964).
[41] R. Laiho, E. Lähderanta, E. Supponen, and L. Vlasenko, Phys. Rev. B **41**, 7674 (1990).
[42] B. Gotschy, G. Denninger, H. Obloh, W. Wilkening, and J. Schneider, Solid State Commun. **71**, 629 (1989).
[43] S. D. Lester, T. S. Kim, and B. G. Streetman, Appl. Phys. Lett. **52**, 474 (1988).
[44] W. Mönch, in *Semiconductor Surfaces and Interfaces*, 2nd ed., edited by G. Ertl, Springer Series in Surface Sciences, Vol. 26 (Springer, Berlin, 1995).
[45] I. Ya. Karlik, D. N. Mirlin, and V. F. Sapega, Fiz. Tverd. Tela (Leningrad) **27**, 2210 (1985) [Sov. Phys. Solid State **27**, 1326 (1985)].
[46] M. A. Alekseev, I. Ya. Karlik, I. A. Merkulov, D. N. Mirlin, and V. F. Sapega, Phys. Lett. A **127**, 373 (1988).
[47] C. Benoitá la Guillaume, J. Phys. Colloq. **35**, C3-1 (1974).
[48] R. R. Parsons, Can. J. Phys. **49**, 1850 (1971).
[49] H. Krenn, K. Kaltenegger, and G. Bauer, *18th International Conference on the Physics of Semiconductors* (World Scientific, Singapore, 1986), pp. 1477–1480.
[50] H. Krenn, K. Kaltenegger, T. Dietl, J. Spalek, and G. Bauer, Phys. Rev. B **39**, 10 918 (1989).
[51] R. Cuscó, J. Ibáñez, and L. Artús, Phys. Rev. B **57**, 12 197 (1998).
[52] A. Debernardi, Phys. Rev. B **57**, 12 847 (1998).
[53] *Semiconductors: Group IV Elements and III-V Compounds*, Data in Science and Technology, edited by O. Madelung (Springer-Verlag, Berlin, 1991).
[54] K. Pressel, K. Thonke, A. Dörnen, and G. Pensl, Phys. Rev. B **43**, 2239 (1991).